DOI: 10.1002/chem.200903476

Asymmetric Hydrogenation with Highly Active IndolPhos–Rh Catalysts: Kinetics and Reaction Mechanism

Jeroen Wassenaar,[a] Mark Kuil,[b] Martin Lutz,[c] Anthony L. Spek,[c] and Joost N. H. Reek*[a]

Abstract: The mechanism of the IndolPhos–Rh-catalyzed asymmetric hydrogenation of prochiral olefins has been investigated by means of X-ray crystal structure determination, kinetic measurements, high-pressure NMR spectroscopy, and DFT calculations. The mechanistic study indicates that the reaction follows an unsaturate/dihydride mechanism according to Michaelis–Menten kinetics. A large value of K_M ($K_M = 5.01 \pm 0.16$ M) is obtained, which indicates that the Rh–solvate complex is the catalyst resting state, which has been observed by high-pressure NMR spectroscopy. DFT calculations on the substrate–catalyst complexes, which are undetectable by experimental means, suggest that the major substrate–catalyst complex leads to the product. Such a mechanism is in accordance with previous studies on the mechanism of asymmetric hydrogenation reactions with C_1-symmetric heteroditopic and monodentate ligands.

Keywords: asymmetric catalysis · hydrogenation · kinetics · reaction mechanisms · rhodium

Introduction

The amplification of chirality by means of asymmetric catalysis is an elegant and useful concept in the synthesis of complex structures, expressing biological activity relevant to pharmaceutical use.[1] Homogeneous transition-metal catalysis has emerged in the past four decades as one of the most efficient and powerful tools to transfer chirality from catalyst to product. Asymmetric hydrogenation (AH) of olefins was found as one of the first catalytic asymmetric reactions, and is still one of the most important industrial processes in the production of chiral fine chemical building blocks.[2] The first catalysts were derived from cationic rhodium and chiral mono- or bidentate phosphorous ligands, which play a pivotal role in obtaining high selectivities, introduced by Knowles and Kagan in the early 1970s.[3] Over the subsequent decades more than three thousand chiral phosphorous ligands have been developed guided by an increasing understanding of the reaction mechanism.[4]

In the seminal work by Halpern[5] and Brown[6] it was proposed that the enantioselectivity in the AH of olefins, in particular, N-acylated dehydroamino esters, is determined by the oxidative addition of dihydrogen to one of the diastereomeric catalyst–substrate complexes **1B** (Scheme 1, top). The less stable diastereomer is more reactive and leads to the product. This so-called "unsaturate/dihydride" mechanism is shown to be operative for C_2-symmetric diphosphines, such as 2,2′-bis(diphenylphosphino)-1,1′-binaphthyl (BINAP), ethylenebis[(2-methoxyphenyl)phenylphosphine] (DIPAMP), and 2,3-bis(diphenylphosphino)butane (CHIRAPHOS). More recently, an alternative mechanism has been proposed by Gridnev and Imamoto for *t*Bu-BisP*–Rh catalysts, which involves oxidative addition of H_2 to the solvate complex **A** prior to alkene coordination ("dihydride/unsaturate" mechanism; Scheme 1, bottom).[7] The enantioselectivity is determined in the migratory insertion of one of the hydrides into the double bond of the substrate. In this case, two possible diastereomeric substrate–RhH_2 complexes

[a] J. Wassenaar, Prof. Dr. J. N. H. Reek
Supramolecular & Homogeneous Catalysis
van 't Hoff Institute for Molecular Sciences'
University of Amsterdam, Nieuwe Achtergracht 166
1018 WV Amsterdam (The Netherlands)
Fax: (+31) 20 5255604
E-mail: J.N.H.Reek@uva.nl

[b] Dr. M. Kuil
BASF Nederland B.V. Catalysts
Strijkviertel 67, 3454 PK De Meern (The Netherlands)
Current address: Solvay Pharmaceuticals

[c] Dr. M. Lutz, Prof. Dr. A. L. Spek
Crystal and Structural Chemistry
Bijvoet Centre for Biomolecular Research
Faculty of Science, Utrecht University
Padualaan 8, 3584 CH Utrecht (The Netherlands)

Supporting information for this article is available on the WWW under http://dx.doi.org/10.1002/chem.200903476.

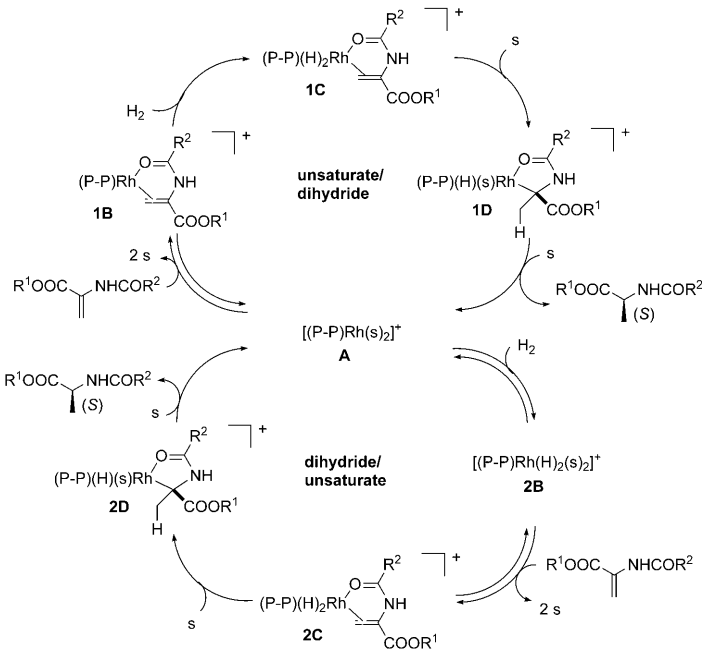

Scheme 1. Unsaturate/dihydride mechanism for the AH of N-acylated dehydroamino esters (P-P = (*R*,*R*)-DIPAMP, (*R*,*R*)-CHIRAPHOS, or (*R*)-BINAP; s = solvent) (top). Dihydride/unsaturated mechanism (P-P = (*R*,*R*)-*t*Bu-BisP*) (bottom).

2C may be formed. Conversely to the unsatuated/dihydride mechanism, the most stable diastereomer leads to the product. In terms of efficiency, the latter mechanism seems attractive as most of the catalyst is involved in the turnover of substrates to products, whereas in the unsaturated/dihydride mechanism only a small fraction of the catalyst participates in turnover, which gives rise to lower reaction rates when the equilibrium between the diastereomeric substrate–catalyst complexes is slow. In addition to these two general mechanisms, highly functionalized ligands can give rise to alternative pathways.[8]

Heteroditopic C_1-symmetric ligands enable desymmetrization of the coordination sphere by differences in the *trans* influence of the donor atoms. As a result, specific substrate coordination is feasible and the exclusion of one diastereomer (**1B** or **2C**) can be achieved. Evans et al. demonstrated this concept by using a P/S mixed ligand.[9] The mechanism in that case follows the unsaturate/dihydride catalytic cycle; however, the stereochemistry of the product suggests that the major diastereomer leads to the product (lock-and-key mechanism). Mechanistic studies by Reetz et al. also indicate a similar mechanism for monodentate phosphite ligands.[10,11]

Hybrid phosphine–phosphoramidite ligands, which also feature heteroditopicity and C_1 symmetry, have been successfully employed to generate highly active and selective catalysts for the AH of functionalized alkenes.[12,13] It has been suggested that these ligands too enable specific substrate binding; however, up to now no detailed mechanistic studies have been reported substantiating this proposition and one may wonder whether the difference in the *trans* influence between phosphine and phosphoramidite allows for such effects. Our laboratory reported the synthesis of phosphine–phosphoramidite IndolPhos (**3**) and its use as a ligand in highly selective asymmetric hydrogenations, hydroformylations, and allylic alkylations.[14] In this report, we investigate the mechanism of the IndolPhos–Rh-catalyzed AH to answer the question of which mechanism is operable, and if specific substrate binding (lock-and-key mechanism) is indeed achieved. The latter will be substantiated by X-ray crystal structure determination, kinetic studies, high-pressure NMR spectroscopy, and DFT calculations.

Results and Discussion

Ligand synthesis: The IndolPhos ligands **3a–f** are synthesized according to the previously reported procedures outlined in Scheme 2.[14a–b] The 2-lithioindole, generated by in

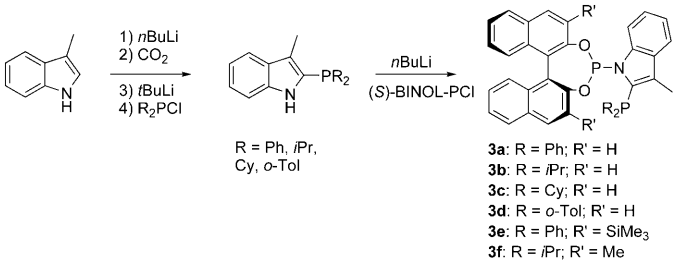

Scheme 2. Synthesis of IndolPhos ligands **3a–f**. (*S*)-BINOL-PCl = (*S*)-(−)-1,1-bi(2-naphthol)phosphorochloridite.

situ protection with CO_2 of the indole NH and subsequent lithiation with *t*BuLi, is reacted with the appropriate phosphine chloride. Condensation of the thus obtained indolylphosphines with (*S*)-bisnaphthol phosphorochloridites gives IndolPhos ligands in good to excellent yield.

X-ray crystal structure: Ligand **3e** was reacted with dichloro-1,5-cyclooctadiene rhodium dimer, and treated subsequently with silver tetrafluoroborate to obtain complex **4** of the formula [Rh(**3e**)(cod)]BF_4 (cod = 1,5-cyclooctadiene).[14a] Crystals suitable for single-crystal X-ray diffraction were obtained as red cubes by slow diffusion of hexane into a dichloromethane solution. The absolute structure of **4** in the noncentrosymmetric space group $P2_12_12_1$ was reliably determined by using the Flack parameter (see the Experimental Section). Top and side views of displacement ellipsoid plots of complex **4** are shown in Figures 1 and 2, respectively. Relevant bond lengths and angles are listed in the caption of Figure 1.

As expected, complex **4** exhibits a square-planar geometry, placing the substituents on phosphorous above and below the coordination plane. The Rh(1)–P(1) bond length is 0.07 Å shorter relative to the Rh(1)–P(2) bond, which indicates significant π-backdonation in the case of the phos-

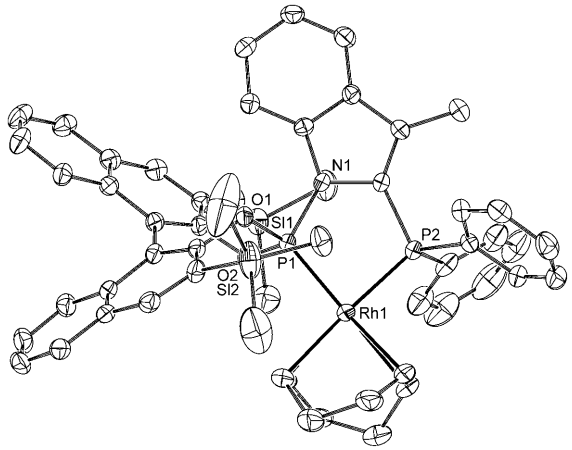

Figure 1. Top view of displacement ellipsoid plot (50% probability level) of complex **4**. Hydrogen atoms, solvent molecules, and the tetrafluoroborate counteranion are omitted for clarity. Selected bond lengths [Å] and angles [°]: Rh(1)–P(1): 2.2152(7), Rh(1)–P(2): 2.2828(7); P(1)-Rh(1)-P(2): 84.75(3).

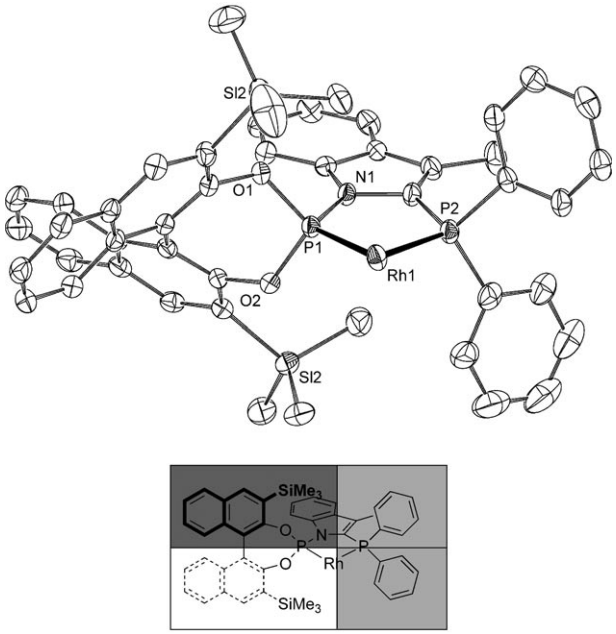

Figure 2. Side view of displacement ellipsoid plot (50% probability level) of complex **4**. Hydrogen atoms, a solvent molecule, the tetrafluoroborate counteranion, and COD are omitted for clarity (top). Quadrant diagram, which indicates the spatial distribution of the steric bulk. Darker regions represent a greater amount of steric crowding (bottom).

phoramidite. Alternatively, the shorter bond length may be explained by less steric crowding in the case of the phosphoramidite, as the substituents point away from the metal compared to the phosphine. The bite angle of 85° is small relative to most chiral bidentate phosphorous ligands. This may explain the high selectivity for the branched aldehyde in the rhodium-catalyzed hydroformylation of styrene, reported earlier.[14a]

The view presented in Figure 2 allows for the construction of a quadrant model. On the right side, intermediate steric crowding is encountered from the substituents on the phosphine. The upper left quadrant exhibits most crowding due to the chiral bisnaphthol moiety. Consequently, the lower left quadrant is most accessible to the bulk solution. Furthermore, it is noteworthy that the aromatic six-membered ring of the indole backbone in part enforces the twisted conformation of the bisnaphthol and further rigidifies the structure. This element of ligand design may be vital to obtain the high selectivities reported in this paper.

Scope of the IndolPhos–Rh-catalyzed hydrogenation: Table 1 summarizes the full substrate scope of the IndolPhos–Rh catalysts. High efficiencies are obtained for *N*-

Table 1. Scope of IndolPhos–Rh-catalyzed AH.[a]

Entry	Ligand	Substrate	Conv. [%]	*ee* [%] (configuration)
1	**3f**	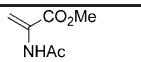	100	97 (*R*)
2	**3f**	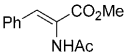	100	97 (*R*)
3	**3b**	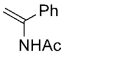	100	94 (*S*)
4	**3f**	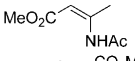	100	99 (*R*)
5	**3a**	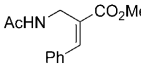	38	87 (nd)[b]
6	**3b**	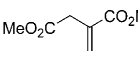	100	98 (*S*)
7[c]	**3b**	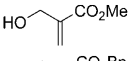	100	98 (*S*)
8	**3b**	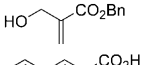	100	89 (*S*)
9	**3f**	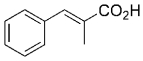	45	78 (*R*)
10	**3f**	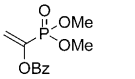	100	87 (*S*)
11	**3a**	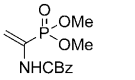	100	55 (*S*)

[a] Reactions were performed in CH_2Cl_2, Rh/L 1:1.1, Rh/substrate 1:100, 10 bar of H_2, at 25 °C for 16 h by using $[Rh(nbd)_2]BF_4$ as the metal precursor. [b] nd = not determined. [c] $T = -40$ °C.

acyl-protected enamides (Table 1, entries 1–5), which allow for the synthesis of protected α- and β-amino acids, and optically active arylamines.[14d] Also double bonds that are not part of an enamide, are hydrogenated efficiently with high enantioselectivity (entries 6–9). In addition to dimethylitaconate, 2-hydroxymethylacrylates giving Roche ester derivatives,[15] which serve as valuable building blocks in natural product synthesis, are hydrogenated in high yield and enantioselectivity (entries 7 and 8).[14b] The functional-group tolerance of the catalytic system is illustrated by the hydrogenation of α-methylcinnamic acid in good enantiomeric excess (*ee*) (entry 9). However, the conversion is decreased

and gas-uptake measurements suggest deactivation of the catalyst over time. Finally, enol- and enamido phosphonate esters are hydrogenated to the corresponding hydroxy- and amino phosphonates quantitatively in moderate to good *ee* (entries 10 and 11).[14d] For most substrates, ligands containing an isopropylphosphine give the highest *ee* values.

Kinetics: To investigate the mechanism of the IndolPhos–Rh AH, a kinetic study was carried out. These kinetic experiments were carried out in the AMTEC SPR16 consisting of 16 parallel reactors equipped with temperature and pressure sensors, and a mass flow controller, allowing the reaction rates to be determined from gas-uptake profiles. We focused our studies on the AH of methyl 2-acetamidoacrylate (MAA) by using the catalyst generated in situ from ligand **3 f** and $[Rh(nbd)_2]BF_4$ (nbd = 2,5-norbornadiene).

Initial rate-determination experiments revealed the high activity of the catalytic system. This required us to lower the catalyst loading to 0.01–0.05 mol%, which resulted in complete conversion after 5 min at room temperature and 10 bar H_2 (see the Supporting Information). In addition, gas-uptake profiles reveal no induction period, which suggests very rapid activation of the precatalyst by hydrogenation of the diolefin. By using Blackmond's kinetic analysis,[16] product inhibition or catalyst decomposition was observed at higher conversions, which required us to determine the rate at an early stage of the reaction. Rate-determination from the gas-uptake profiles allowed us to determine the order in the Rh catalyst from a ln[Rh]/ln(TOF) plot (Figure 3). A first order is obtained from the slope of this plot, which is expected for a mononuclear Rh-catalyzed AH mechanism. Absolute turnover frequencies of over 90,000 h^{-1} are achieved by this catalytic system.

Next, we determined the order in olefin concentration at S/C ratios of 1250–2500 (Figure 4). The ln[olefin]/ln(TOF) plot yields a straight line with slope = 1, indicative of a first-order reaction. A first-order dependency on the substrate concentration is rarely observed for AH of olefins,[17] as the oxidative addition of dihydrogen is proposed to be the rate-limiting step. In these cases, Michaelis–Menten kinetics are proposed to be operable, in which the pre-equilibrium forming the catalyst–substrate complex lies on the side of the educts (vide infra). To arrive at saturation kinetics, we conducted rate measurements at higher S/C ratios of 3400–5600. Indeed, the order in the olefin concentration is lowered to approximately 0.5, which indicates that the pre-equilibrium is shifted (Figure 5). Unfortunately, further lowering of the amount of catalyst resulted in loss of activity, which is tentatively ascribed to very small impurities in the substrate that poison the catalyst (note: at S/C ratios of over 10,000, the purity of the substrate has to exceed 99.9999%).

Due to the limitations of the MAA system, we decided to perform a full reaction progress kinetic analysis of the AH of dimethyl itaconate (DMI) by using ligand **3b**. Previous studies by Heller and co-workers have shown that this substrate shows similar behavior in asymmetric hydrogenation relative to dehydroamino acid esters.[18] Indeed, in this case we were able to lower the catalyst loading to an S/C ratio of 30,000, presumably because of lower levels of impurities in this substrate. The corresponding graphical rate equation is depicted in Figure 6.

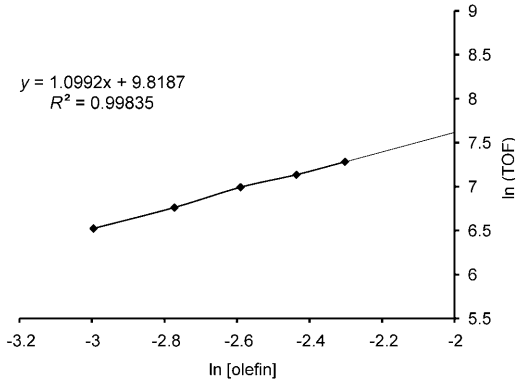

Figure 4. Ln[olefin]/ln(TOF) plot for the AH of MAA by [Rh(**3 f**)-(nbd)]BF_4 at S/C ratios between 1250–2500 and 10 bar H_2 ([olefin] in M, TOF in mol mol^{-1} min^{-1}).

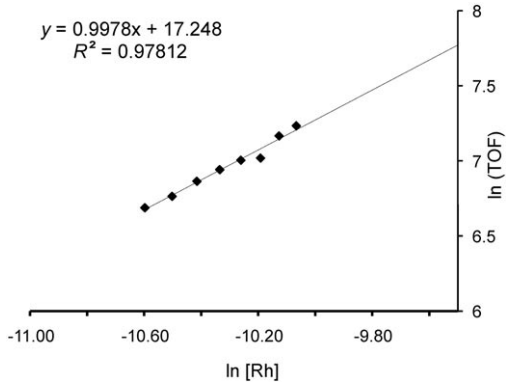

Figure 3. Ln[Rh]/ln(TOF) plot for the AH of MAA by [Rh(**3 f**)(nbd)]BF_4 at S/C ratios of 4000–8000 and 10 bar H_2 ([Rh] in M, TOF in mol mol^{-1} min^{-1}.

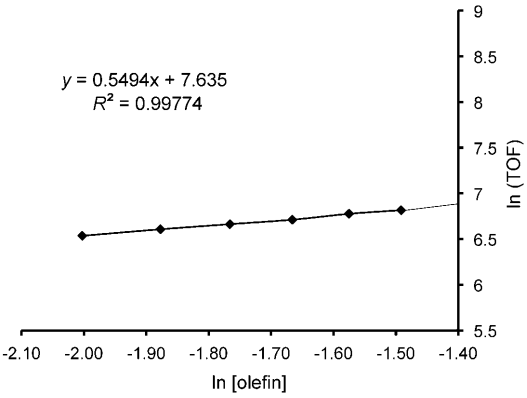

Figure 5. Ln[olefin]/ln(TOF) plot for the AH of MAA by [Rh(**3 f**)-(nbd)]BF_4 at S/C ratios between 3400–5600 and 10 bar H_2 ([olefin] in M, TOF in mol mol^{-1} min^{-1}).

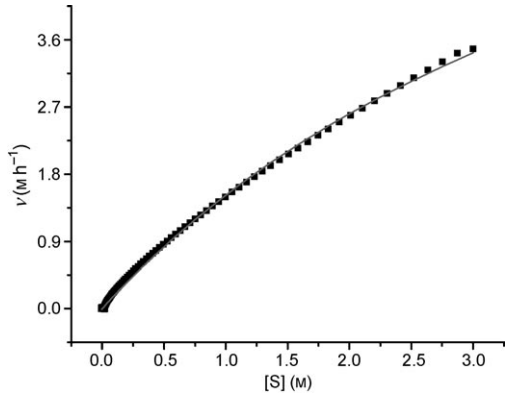

Figure 6. Rate versus substrate concentration plot for the AH of DMI by [Rh(**3b**)(nbd)]BF_4; a fit to Equation (1) gives $k_2 = 9.14 \pm 0.21\,\text{M h}^{-1}$ and $K_M = 5.01 \pm 0.16\,\text{M}$.

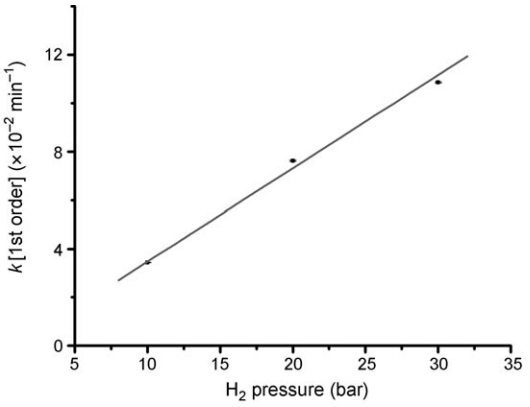

Figure 8. Plot of first-order rate constants versus hydrogen pressure for the AH of DMI by [Rh(**3b**)(nbd)]BF_4.

The plot of reaction rate versus substrate concentration shows a strong, almost linear dependency. Therefore, for substrate concentrations below 3 M, a first order approximation for the rate equation may be used. The influence of catalyst concentration and hydrogen pressure were thus determined by using first-order rate constants obtained by a fitting of the experimental curves to a first-order function (Figures 7 and 8). Both plots reveal, as expected, a first-order

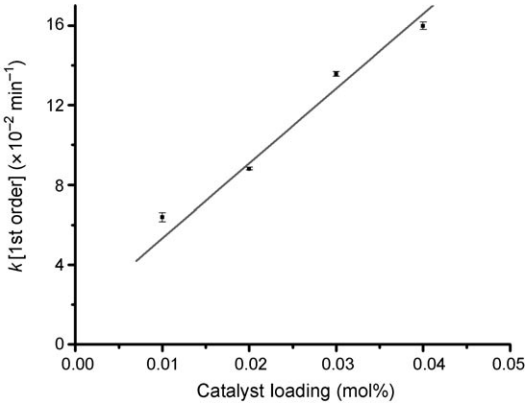

Figure 7. Plot of first-order rate constants versus catalyst loading for the AH of DMI by [Rh(**3b**)(nbd)]BF_4.

dependency of the reaction on the amount of catalyst and hydrogen pressure. For dimethyl itaconate, very high initial turnover frequencies are obtained ($> 50\,000\,\text{h}^{-1}$) and turnover numbers up to 30,000.

The kinetics of the AH of MAA and dimethyl itaconate by IndolPhos–Rh catalysts can best be described by Michaelis–Menten kinetics as was shown previously for diphosphine systems by following the unsaturate/dihydride pathway.[5b,d,19] In this Michaelis–Menten model, reversible coordination of the alkene forming the diastereomeric substrate–catalyst complexes **1B**, is followed by an irreversible reaction with dihydrogen. The irreversible rate-determining step may then be either oxidative addition of dihydrogen or migratory insertion (see Figure S-1 in the Supporting Information). The rate equation can, under isobaric conditions ($k_2 = k_2'\,[H_2]$), be written as depicted in Equation (1), and two limiting cases can be distinguished. If the olefin concentration is very high, the pre-equilibrium is completely shifted towards the catalyst–substrate complex and the rate depends solely on the rhodium (catalyst) concentration and hydrogen pressure [Eq. (2)]. On the other hand, at lower olefin concentrations the rate also depends linearly on the substrate concentration [Eq. (3)]. The absolute values of these concentrations are determined by the magnitude of K_M [Eq. (4)].

$$v = \frac{d[P]}{dt} = \frac{k_2[Rh]_0[S]}{K_M + [S]} \quad (1)$$

$$\frac{d[P]}{dt} = k_2[Rh]_0 \quad \text{for } K_M \ll [S] \quad (2)$$

$$\frac{d[P]}{dt} = \frac{k_2[Rh]_0}{K_M}[S] = k_{obs}[S] \quad \text{for } K_M \gg [S] \quad (3)$$

$$K_M = \frac{[\mathbf{A}][S]}{[\mathbf{1B}]} \quad (4)$$

The kinetic profiles for the hydrogenation of MAA and dimethyl itaconate indicate that under typical conditions, the reaction exhibits first-order behavior [Eq. (3)]. For dimethyl itaconate, values for k_2 and K_M could be obtained from the graphical rate equation by fitting the data to Equation (1) (Figure 6). The very high value of K_M ($K_M = 5.01 \pm 0.16\,\text{M}$) indicates that most of the catalyst is present as the solvent complex, that is, the resting state of the catalyst. The measured value for K_M is unusually high for AH reactions, which generally exhibit zero-order kinetics and the substrate–catalyst complexes **1B** are the resting state. Alternatively, the mechanism may follow a dihydride/unsaturated pathway in which the rate-determining step is the coordination of the alkene to the solvate–dihydride complex **2B** or subsequent migratory insertion (see Figure S-2 in the Sup-

porting Information). However, the inability to detect solvate–dihydride species by high-pressure NMR spectroscopy speaks against this (vide infra).

High-pressure NMR spectroscopy: The kinetic experiments described above give valuable information about the rate equation; however, it does not allow for detection of the intermediates in the catalytic cycle. We therefore turned to high-pressure NMR spectroscopy to obtain structural information about these intermediates. Also for these studies we used the in situ generated complex $[Rh(\mathbf{3f})(nbd)]BF_4$ (**5**), which exhibits two doublets-of-doublets in the ^{31}P NMR spectrum at $\delta = 141$ and 54 ppm with $J_{PP} = 52.7$ Hz. When this complex is subjected to five bar pressure of molecular hydrogen in CD_2Cl_2, very broad signals are obtained. However, when this species is reacted with alkene substrates, the hydrogenation products were obtained with the same enantioselectivity. Addition of MeCN to this ill-defined species yields the MeCN solvate complex, $[Rh(\mathbf{3f})(MeCN)_2]BF_4$, which indicates that the species giving broad signals is the CD_2Cl_2 solvent complex. Formation of the well-defined solvate complex $[Rh(\mathbf{3f})(CD_3OD)_2]BF_4$ is also achieved by changing the solvent to deuteromethanol, characterized by a new set of doublets-of-doublets at $\delta = 146.4$ and 78.4 ppm with $J_{PP} = 72.4$ Hz. Attempts to detect the solvate–dihydride complex **2B** at low temperatures by following the protocol by Gridnev and Imamoto were unsuccessful.[7a] Furthermore, efforts to replace solvent molecules with substrates did not result in the formation of diastereomeric catalyst–substrate complexes **1B**, which is in line with the kinetic profile (K_M is very large).

The high-pressure NMR spectroscopic experiments are in agreement with the kinetic data as no substrate–catalyst complexes could be obtained. Instead, stable solvate complexes could be detected, representing the major resting state. The inability of the solvate complexes to form dihydrides at low temperatures indicates that an unsaturate/dihydride pathway is followed. Recent contributions from Gridnev and Imamoto suggest that dihydride formation may be accelerated by partial substrate coordination through the carbonyl function.[7d] This may indeed also occur in our system under catalytic conditions, but we are unable to study this as no substrate–catalyst complexes can be prepared.

DFT calculations: The kinetic studies in conjunction with the high-pressure NMR spectroscopic studies discussed above point towards an unsaturate/dihydride pathway in which the absolute configuration of the product is determined in the oxidative addition of dihydrogen to one of the catalyst–substrate complexes **1B**. As these species cannot be detected experimentally because of the large value of K_M, we decided to calculate the four possible diastereomeric catalyst–substrate complexes **1B** at a high level of theory (B3LYP, 6-31G*/LANL2DZ) without any constraints, for the hydrogenation of dimethyl itaconate, by using ligand **3b**. The obtained structures and energies are depicted in Figure 9.

The calculations indicate that one complex, pro-(*S*)-*trans*-**1B**, appears to be much more stable than the other three complexes. The greater stability can be understood in terms of perturbation from the ideal square-planar geometry preferred by Rh^I and the *trans* effect. In the case of pro-(*R*)-*trans*-**1B**, the alkene is tilted out of the coordination plane because of steric repulsion of the α,β-unsaturated ester with the bisnaphthol moiety, forcing the methyl group of the ester to be eclipsing with the alkene fragment. Complex pro-(*S*)-*cis*-**1B** also displays out of plane coordination of the alkene; however, in this case caused by repulsive interactions between the saturated ester and the bisnaphthol fragment. For pro-(*R*)-*cis*-**1B**, the orientation of the substrate causes steric crowding between the α,β-unsaturated ester and the bisnaphthol group and the phosphine–carbonyl *trans* disposition is less favorable relative to the phosphoramidite–carbonyl *trans*.

We found experimentally that the *S* enantiomer is obtained in an excellent *ee* of 98% by using ligand **3b**. This result is in good agreement with the outcome of the DFT calculations, which predict that the diastereoisomer pro-(*S*)-*trans*-**1B**, leading to the *S*-enantiomer is the only populated one at room temperature according to the Boltzmann distribution. It is possible that alkene decoordination may occur during the oxidative addition step as proposed by Gridnev and Imamoto (vide supra). Therefore, a full computational analysis of the reaction pathway is necessary to substantiate the true origin of enantioselection. However, theory and experiment are in good agreement and suggest that the major substrate–catalyst complex leads to the product in the IndolPhos-catalyzed AH of dimethyl itaconate and most probably also for other substrates coordinating in a similar fashion.

The proposed mechanism differs significantly to the Halpern and Brown mechanism for C_2-symmetric diphosphines, in which the least-stable diastereomeric substrate–catalyst complex leads to the product (vide supra). Landis and coworkers calculated the whole reaction pathway of the rhodium-catalyzed AH, by using DuPHOS as the chiral ligand.[20] They found energy differences between the major and minor catalyst substrate complexes of 3.7 kcal mol^{-1} and a total energy difference between the two pathways of 4.4 kcal mol^{-1}. In our case, the energy differences in the substrate–catalyst complexes are much larger (9.4 kcal mol^{-1}) at the same level of theory. In addition, the overall reaction activation energy (E_a) is approximately 15.3 kcal mol^{-1} for the hydrogenation of DMI, which is derived from the value of k_2 by using the Arrhenius equation. Consequently, a mechanism similar to the one proposed by Evans and Reetz for C_1-symmetric P/S and monodentate ligands is much more likely to be operable for IndolPhos–Rh catalysts.[9,10]

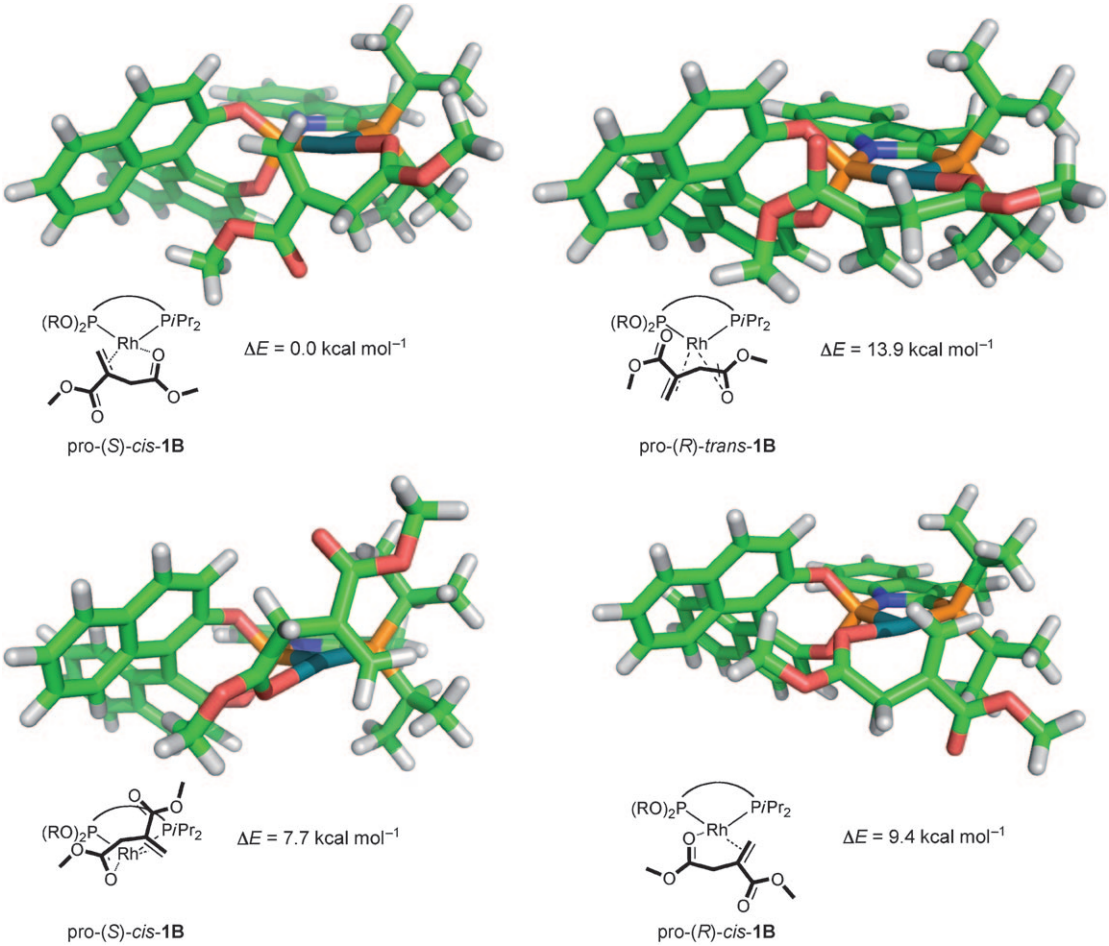

Figure 9. Calculated (B3LYP, 6-31G*/LANL2DZ) structures and energies of diastereomeric catalyst–substrate complexes **1B**.

Conclusion

IndolPhos–Rh complexes are shown to be highly active (TOF > 90,000 h^{-1}) and enantioselective (up to 99% *ee*) hydrogenation catalysts for a broad range of prochiral alkenes, making them suitable candidates for industrial large scale AH processes.[21] Their facile preparation allows for easy derivatization leading to a rapid construction of a small ligand library. Kinetic studies indicate that the AH of MAA and dimethyl itaconate follows Michaelis–Menten kinetics, exhibiting a very large value for K_M, which indicates that the Rh–solvate complex is the major resting state of the catalyst. Several solvate complexes have been observed by high-pressure NMR spectroscopy and form neither substrate–catalyst complexes nor solvate–dihydride species. This suggests that an unsaturate/dihydride mechanism is followed, but we cannot exclude a dihydride/unsaturate mechanism completely. High-level DFT calculations indicate that only one of four diastereomeric substrate–catalyst complexes is energetically accessible, which leads to the experimentally found absolute configuration of the product. We are currently investigating the full reaction pathway by DFT calculations to substantiate these findings.

In conclusion, the mechanistic studies on IndolPhos–Rh catalysts reported in this paper are in line with a lock-and-key type mechanism of enantiodiscrimination as has been previously proposed for C_1-symmetric P/S and monodentate ligands.[9,10] However, on the basis of the current data we cannot exclude other mechanistic pathways. Relative to the anti-lock-and-key mechanism observed for C_2-symmetric ligands, this mechanism is more elegant and efficient as the major flux of the reaction proceeds through the major isomer, that is, a higher effective catalyst concentration. For IndolPhos–Rh catalysts, however, a large amount of the catalysts exists as the solvate complex at typical conditions.

Experimental Section

Kinetic gas-uptake measurements: The experiments were carried out in an AMTEC SPR16 consisting of 16 parallel reactors equipped with temperature and pressure sensors, and a mass flow controller. The apparatus is suited for monitoring gas-uptake profiles during the catalytic reactions. The autoclaves were heated to 110 °C and flushed with argon (22 bar) five times. Next, the reactors were cooled to 25 °C and flushed again with argon (22 bar) five times. The autoclaves were charged with the appropriate amount of $[Rh(nbd)_2(BF_4)]$, ligand **3**, and substrate in CH_2Cl_2

(8.00 mL) under argon. The reactors were pressurized to the desired pressure with H_2 and the pressure was kept constant during the whole reaction. The reaction mixtures were stirred at 25 °C and the hydrogen uptake was monitored and recorded for every reactor. After catalysis, the pressure was reduced to 2.0 bar and samples (0.2 mL) were taken for chiral GC analysis.

High-pressure NMR spectroscopic experiments: In a typical experiment, a 5 mm sapphire high-pressure NMR spectroscopic tube was filled with a solution of $[Rh(nbd)_2]BF_4$ (5.6 mg, 0.015 mmol), ligand **3f** (8.8 mg, 0.015 mmol), and CD_2Cl_2 or CD_3OD (0.5 mL). The tube was purged three times with 5 bar of H_2, and then pressurized with 5 bar of H_2. After vigorous manual shaking for approximately 2 min, the tube was inserted in the NMR spectrometer.

[Rh(3f)(CD$_3$OD)$_2$]BF$_4$: ^{1}H NMR (500 MHz, CD_3OD, 253 K): $\delta = 8.15$ (s, 1H), 8.06 (d, $J = 8.3$ Hz, 1H), 7.92 (d, $J = 8.3$ Hz, 1H), 7.82–7.79 (m, 2H), 7.63 (d, $J = 8.0$ Hz, 1H), 7.51 (d, $J = 7.8$ Hz, 1H), 7.13–7.09 (m, 1H), 6.98 (t, $J = 7.6$ Hz, 1H), 6.89 (d, $J = 8.3$ Hz, 1H), 6.17 (t, $J = 7.5$ Hz, 1H), 6.01 (t, $J = 1.8$ Hz, 2H), 5.88 (d, $J = 8.4$ Hz, 1H), 3.09 (s, 3H), 2.85 (m, 3H), 1.66–1.64 (m, 2H), 1.62 (s, 3H), 1.52–0.93 ppm (m, 12H); ^{31}P NMR (202 MHz, CD_3OD): $\delta = 146.43$ (dd, $J = 331.8$, 72.6 Hz, 1P), 78.42 ppm (dd, $J = 180.3$, 72.3 Hz, 1P).

[Rh(3b)(MeCN)$_2$]BF$_4$: Ligand **3b** (100 mg, 0.18 mmol) was added to solution of $[Rh(nbd)_2]BF_4$ (67 mg, 0.18 mmol) in CH_2Cl_2 (4 mL) and stirred for 30 min at RT. Dihydrogen was bubbled through the solution for 30 min. Filtration through Celite followed by evaporation of the solvent in vacuo. Washing of the resulting orange solid with hexane (3×5 mL) and drying in vacuo gave the characteristic broad NMR spectra for the CH_2Cl_2–solvate complex. The compound was redissolved in MeCN (5 mL), stirred for 20 min at RT, and the solvent was removed in vacuo to give a yellow solid. The solid can be handled in air but decomposes overnight in $CDCl_3$ and upon storage in air for several days. Yield: 122 mg (82%); ^{1}H NMR (500 MHz, $CDCl_3$, 298 K): $\delta = 8.16$ (d, $J = 8.8$ Hz, 1H), 8.02 (d, $J = 8.2$ Hz, 1H), 7.92 (d, $J = 8.1$ Hz, 1H), 7.76 (d, $J = 8.8$ Hz, 1H), 7.71 (d, $J = 8.8$ Hz, 1H), 7.54–7.50 (m, 2H), 7.43–7.32 (m, 5H), 6.99 (t, $J = 7.5$ Hz, 1H), 6.92 (d, $J = 8.8$ Hz, 1H), 6.37 (t, $J = 7.8$ Hz, 1H), 6.00 (d, $J = 8.5$ Hz, 1H), 2.68 (2×td, $J = 15.3$, 7.8 Hz, 2H), 2.43 (s, 3H), 2.14 (brs, 6H), 1.49–1.33 (m, 9H), 1.17 ppm (dd, $J = 16.9$, 6.9 Hz, 3H); ^{13}C NMR (126 MHz, $CDCl_3$, 298 K): $\delta = 149.63$ (d, $J = 16.0$ Hz), 147.70 (d, $J = 5.2$ Hz), 136.86 (d, $J = 6.9$ Hz), 132.68 (s), 132.33 (s), 131.86 (s), 131.57 (s), 131.22 (s), 130.71 (s), 128.55 (d, $J = 3.1$ Hz), 127.22 (s), 127.05 (s), 127.02 (s), 126.95 (s), 126.33 (s), 125.81 (s), 124.39 (s), 123.27 (d, $J = 1.9$ Hz), 122.99 (s), 122.34 (s), 121.46 (s), 121.10 (s), 119.55 (s), 115.28 (s), 70.68 (s), 27.52 (d, $J = 8.7$ Hz), 27.29 (d, $J = 10.7$ Hz), 26.61 (s), 20.23 (s), 20.08 (d, $J = 4.5$ Hz), 19.99 (s), 19.82 (d, $J = 4.5$ Hz), 11.13 (s), 2.26 ppm (s); ^{31}P NMR (202 MHz, $CDCl_3$, 298 K): $\delta = 148.45$ (dd, $J = 294.5$, 63.1 Hz; 1P), 71.60 ppm (dd, $J = 159.2$, 63.0 Hz; 1P); MS (ESI) m/z: calcd for $C_{39}H_{39}N_3O_2P_2Rh$: 746.16 $[M-BF_4]^+$; found: 746.20.

X-ray crystal-structure determination of 4: $[C_{55}H_{57}NO_2P_2RhSi_2](BF_4)\cdot CH_2Cl_2$ + disordered solvent; $F_w = 1156.78$; orange block; 0.25×0.12×0.09 mm^3; orthorhombic; $P2_12_12_1$ (no. 19); $a = 14.1237(1)$, $b = 15.3310(1)$, $c = 26.7687(2)$ Å; $V = 5796.24(7)$ Å^3; $Z = 4$; $D_x = 1.33$ g cm^{-3}; $\mu = 0.54$ mm^{-1}.[1] 74726 reflections were measured on a Nonius Kappa CCD diffractometer with rotating anode (graphite monochromator, $\lambda = 0.71073$ Å) up to a resolution of $(\sin\theta/\lambda)_{max} = 0.65$ Å^{-1} at a temperature of 150(2) K. Intensities were integrated with HKL2000.[22]. An absorption correction based on multiple measured reflections was performed by using the program SADABS[23] (correction range 0.74–0.95). 13196 reflections were unique ($R_{int} = 0.041$), of which 11865 were observed [$I > 2\sigma(I)$]. The structure was solved with direct methods by using the program SHELXS-97.[24] The structure was refined with SHELXL-97[24] against F^2 of all reflections. Non-hydrogen atoms were refined with anisotropic displacement parameters. All hydrogen atoms were introduced in calculated positions and refined with a riding model. The crystal structure contains ordered dichloromethane solvent molecules, which were refined with full occupancies. The crystal structure also contains voids (542 Å^3/unit cell) filled with severely disordered dichloromethane molecules. Their contribution to the structure factors was taken into account by using a back-Fourier transformation with the SQUEEZE routine of the program PLATON[25], resulting in 151 electrons/unit cell. 647 parameters were refined with 11 restraints. $R1/wR2$ [$I > 2\sigma(I)$]: 0.0351/0.0840. $R1/wR2$ [all refl.]: 0.0418/0.0871. $S = 1.041$. Flack x-parameter:[26] −0.024(16). Residual electron density between −0.81 and 0.93 e Å^3. Geometry calculations and checking for higher symmetry were performed with the PLATON program.[25]

[1] Derived parameters do not contain the contribution of the disordered solvent.

CCDC-756580 contain the supplementary crystallographic data for this paper. These data can be obtained free of charge from The Cambridge Crystallographic Data Centre via www.ccdc.cam.ac.uk/data_request/cif.

Computational details: DFT calculations were performed by using the Spartan '04 for windows program package,[27] employing the B3LYP functional.[28] The basis set was 6–31G* for all atoms,[29] except for Rh, which was described by an effective core potential and the associated basis set LANL2DZ.[30] Graphics were generated by using MacPyMOL.[31]

Acknowledgements

This work was supported by the NRSC-C and the European Union (RTN Revcat MRTN-CT-2006-035866). We thank R.J. Detz for assistance with the AMTEC experiments. This work was also supported in part (M.L, A.L.S.) by the Council for the Chemical Sciences of The Netherlands Organization for Scientific Research (CW-NWO).

[1] J. S. Carey, D. Laffan, C. Thomson, M. T. Williams, *Org. Biomol. Chem.* **2006**, *4*, 2337–2347.
[2] a) J. G. de Vries, C. J. Elsevier, *The Handbook of Homogeneous Hydrogenation*, Wiley-VCH, Weinheim, **2007**; b) H. U. Blaser, B. Pugin, F. Spindler, M. Thommen, *Acc. Chem. Res.* **2007**, *40*, 1240–1250.
[3] T. Ohkuma, M. Kitamura, R. Noyori in *New Frontiers in Asymmetric Catalysis* (Eds.: K. Mikami, M. Lautens), Wiley, New York, **2007**, pp. 1–32.
[4] W. Tang, X. Zhang, *Chem. Rev.* **2003**, *103*, 3029–3069.
[5] a) A. S. C. Chan, J. Halpern, *J. Am. Chem. Soc.* **1980**, *102*, 838–840; b) A. S. C. Chan, J. J. Pluth, J. Halpern, *J. Am. Chem. Soc.* **1980**, *102*, 5952–5954; c) J. Halpern, *Science* **1982**, *217*, 401–407; d) C. R. Landis, J. Halpern, *J. Am. Chem. Soc.* **1987**, *109*, 1746–1754.
[6] a) J. M. Brown, P. A. Chaloner, *Tetrahedron Lett.* **1978**, *19*, 1877–1880; b) J. M. Brown, P. A. Chaloner, *J. Am. Chem. Soc.* **1980**, *102*, 3040–3048.
[7] a) I. D. Gridnev, N. Higashi, K. Asakura, T. Imamoto, *J. Am. Chem. Soc.* **2000**, *122*, 7183–7194; b) I. D. Gridnev, T. Imamoto, *Acc. Chem. Res.* **2004**, *37*, 633–644; c) I. D. Gridnev, T. Imamoto, *Chem. Commun.* **2009**, 7447–7464; d) I. D. Gridnev, T. Imamoto, G. Hoge, M. Kouchi, H. Takahashi, *J. Am. Chem. Soc.* **2008**, *130*, 2560–2572.
[8] a) F. W. Patureau, M. Kuil, A. J. Sandee, J. N. H. Reek, *Angew. Chem.* **2008**, *120*, 3224–3227; *Angew. Chem. Int. Ed.* **2008**, *47*, 3180–3183; b) F. W. Patureau, S. de Boer, M. Kuil, J. Meeuwissen, P. A. R. Breuil, M. A. Siegler, A. L. Spek, A. J. Sandee, B. de Bruin, J. N. H. Reek, *J. Am. Chem. Soc.* **2009**, *131*, 6683–6685.
[9] D. A. Evans, F. E. Michael, J. S. Tedrow, K. R. Campos, *J. Am. Chem. Soc.* **2003**, *125*, 3534–3543.
[10] M. T. Reetz, A. Meiswinkel, G. Mehler, K. Angermund, M. Graf, W. Thiel, R. Mynott, D. G. Blackmond, *J. Am. Chem. Soc.* **2005**, *127*, 10305–10313.
[11] I. D. Gridnev, C. Fan, P. G. Pringle, *Chem. Commun.* **2007**, 1319–1321.
[12] For reviews, see: a) D. Amoroso, T. W. Graham, R. W. Guo, C. W. Tsang, K. A. Rashid, *Aldrichimica Acta* **2008**, *41*, 15–26; b) F. Boeda, T. Beneyton, C. Crévisy, *Mini-Rev. Org. Chem.* **2008**, *5*, 96–127.
[13] a) G. Franciò, F. Faraone, W. Leitner, *Angew. Chem.* **2000**, *112*, 1486–1488; *Angew. Chem. Int. Ed.* **2000**, *39*, 1428–1430; b) X. P.

Hu, Z. Zheng, *Org. Lett.* **2004**, *6*, 3585–3588; c) X. P. Hu, Z. Zheng, *Org. Lett.* **2005**, *7*, 419–422; d) Q. H. Zeng, X. P. Hu, Z. C. Duan, X. M. Liang, Z. Zheng, *Tetrahedron: Asymmetry* **2005**, *16*, 1233–1238; e) J. D. Huang, X. P. Hu, Z. C. Duan, Q. H. Zeng, S. B. Yu, J. Deng, D. Y. Wang, Z. Zheng, *Org. Lett.* **2006**, *8*, 4367–4370; f) D. Y. Wang, X. P. Hu, J. D. Huang, J. Deng, S. B. Yu, Z. C. Duan, X. F. Xu, Z. Zheng, *Angew. Chem.* **2007**, *119*, 7956–7959; *Angew. Chem. Int. Ed.* **2007**, *46*, 7810–7813; g) M. Qiu, X. P. Hu, D. Y. Wang, J. Deng, J. D. Huang, S. B. Yu, Z. C. Duan, Z. Zheng, *Adv. Synth. Catal.* **2008**, *350*, 1413–1418; h) S. B. Yu, J.-D. Huang, D. Y. Wang, X. P. Hu, J. Deng, Z. C. Duan, Z. Zheng, *Tetrahedron: Asymmetry* **2008**, *19*, 1862–1866; i) K. A. Vallianatou, I. D. Kostas, J. Holz, A. Börner, *Tetrahedron Lett.* **2006**, *47*, 7947–7950; j) Y. Yan, X. Zhang, *J. Am. Chem. Soc.* **2006**, *128*, 7198–7202; k) X. Zhang, B. Cao, Y. Yan, S. Yu, B. Ji, X. Zhang, *Chem. Eur. J.* **2010**, *16*, 871–877; l) Z. C. Duan, X. P. Hu, J. Deng, S. B. Yu, D. Y. Wang, Z. Zheng, *Tetrahedron: Asymmetry* **2009**, *20*, 588–592; m) M. Qiu, D. Y. Wang, X. P. Hu, J. D. Huang, S. B. Yu, J. Deng, Z. C. Duan, Z. Zheng, *Tetrahedron: Asymmetry* **2009**, *20*, 210–213; n) S. B. Yu, X. P. Hu, J. Deng, D. Y. Wang, Z. C. Duan, Z. Zheng, *Tetrahedron: Asymmetry* **2009**, *20*, 621–625.

[14] a) J. Wassenaar, J. N. H. Reek, *Dalton Trans.* **2007**, 3750–3753; b) J. Wassenaar, M. Kuil, J. N. H. Reek, *Adv. Synth. Catal.* **2008**, *350*, 1610–1614; c) J. Wassenaar, S. van Zutphen, G. Mora, P. Le Floch, M. A. Siegler, A. L. Spek, J. N. H. Reek, *Organometallics* **2009**, *28*, 2724–2734; d) J. Wassenaar, J. N. H. Reek, *J. Org. Chem.* **2009**, *74*, 8403–8406.

[15] The name Roche ester, which is nowadays frequently used for (*S*)-3-hydroxy-2-methylpropionate, should not be confused with the Roche company. The name is derived from the university of Rochester (New York, USA) where its synthesis has been described for the first time by Herrmann and Schlessinger, see: J. L. Herrmann, R. H. Schlessinger, *Tetrahedron Lett.* **1973**, *14*, 2429–2432.

[16] D. G. Blackmond, *Angew. Chem.* **2005**, *117*, 4374–4393; *Angew. Chem. Int. Ed.* **2005**, *44*, 4302–4320.

[17] a) D. Heller, R. Kadyrov, M. Michalik, T. Freier, U. Schmidt, H. W. Krause, *Tetrahedron: Asymmetry* **1996**, *7*, 3025–3035; b) H. J. Drexler, A. Preetz, T. Schmidt, D. Heller in *The Handbook of Homogeneous Hydrogenation, Vol. 1* (Eds.: J. G. de Vries, C. J. Elsevier), Wiley-VCH, Weinheim, **2007**, pp. 257–293.

[18] a) H. J. Drexler, S. L. Zhang, A. L. Sun, A. Spannenberg, A. Arrieta, A. Preetz, D. Heller, *Tetrahedron: Asymmetry* **2004**, *15*, 2139–2150; b) H. J. Drexler, W. Baumann, T. Schmidt, S. L. Zhang, A. L. Sun, A. Spannenberg, C. Fischer, H. Buschmann, D. Heller, *Angew. Chem.* **2005**, *117*, 1208–1212; *Angew. Chem. Int. Ed.* **2005**, *44*, 1184–1188; c) A. Preetz, H. J. Drexler, C. Fischer, Z. Dai, A. Börner, W. Baumann, A. Spannenberg, R. Thede, D. Heller, *Chem. Eur. J.* **2008**, *14*, 1445–1451; d) T. Schmidt, Z. Dai, H. J. Drexler, W. Baumann, C. Jager, D. Pfeifer, D. Heller, *Chem. Eur. J.* **2008**, *14*, 4469–4471; e) T. Schmidt, Z. Dai, H. J. Drexler, M. Hapke, A. Preetz, D. Heller, *Chem. Asian J.* **2008**, *3*, 1170–1180; f) T. Schmidt, H. J. Drexler, J. Sun, Z. Dai, W. Baumann, A. Preetz, D. Heller, *Adv. Synth. Catal.* **2009**, *351*, 750–754.

[19] M. Kitamura, M. Tsukamoto, Y. Bessho, M. Yoshimura, U. Kobs, M. Widhalm, R. Noyori, *J. Am. Chem. Soc.* **2002**, *124*, 6649–6667.

[20] a) C. R. Landis, P. Hilfenhaus, S. Feldgus, *J. Am. Chem. Soc.* **1999**, *121*, 8741–8754; b) S. Feldgus, C. R. Landis, *J. Am. Chem. Soc.* **2000**, *122*, 12714–12727; c) C. R. Landis, S. Feldgus, *Angew. Chem.* **2000**, *112*, 2985–2988; *Angew. Chem. Int. Ed.* **2000**, *39*, 2863–2866; d) S. Feldgus, C. R. Landis, *Organometallics* **2001**, *20*, 2374–2386.

[21] H. U. Blaser, F. Spindler, M. Thommen in *The Handbook of Homogeneous Catalysis, Vol. 3* (Eds.: J. G. de Vries, C. J. Elsevier), Wiley-VCH, Weinheim, **2007**, pp. 1279–1324.

[22] Z. Otwinowski, W. Minor in *Methods in Enzymology* (Eds.: C. W. Carter Jr., R. M. Sweet), Academic Press, New York, **1997**, pp. 307–326.

[23] SADABS 2006/1, G. M. Sheldrick, University of Göttingen, Göttingen, **2006**.

[24] G. M. Sheldrick, *Acta Crystallogr. Sect. A* **2008**, *64*, 112–122.

[25] A. L. Spek, *Acta Crystallogr. Sect. D* **2009**, *65*, 148–155.

[26] H. D. Flack, *Acta Crystallogr. Sect. A* **1983**, *39*, 876–881.

[27] Spartan '04 for windows, Wavefunction, Inc., Irvine, California, **2004**.

[28] a) S. H. Vosko, L. Wilk, M. Nusair, *Can. J. Phys.* **1980**, *58*, 1200–1211; b) C. T. Lee, W. T. Yang, R. G. Parr, *Phys. Rev. B* **1988**, *37*, 785–789; c) A. D. Becke, *J. Chem. Phys.* **1993**, *98*, 5648–5652; d) P. J. Stephens, F. J. Devlin, C. F. Chabalowski, M. J. Frisch, *J. Phys. Chem.* **1994**, *98*, 11623–11627.

[29] a) P. C. Hariharan, J. A. Pople, *Theor. Chim. Acta* **1973**, *28*, 213–222; b) M. M. Francl, W. J. Pietro, W. J. Hehre, J. S. Binkley, M. S. Gordon, D. J. Defrees, J. A. Pople, *J. Chem. Phys.* **1982**, *77*, 3654–3665.

[30] P. J. Hay, W. R. J. Wadt, *J. Chem. Phys.* **1985**, *82*, 270; P. J. Hay, W. R. J. Wadt, *J. Chem. Phys.* **1985**, *82*, 284; P. J. Hay, W. R. J. Wadt, *J. Chem. Phys.* **1985**, *82*, 299.

[31] The PyMOL Molecular Graphics System, W. L. DeLano, DeLano Scientific LLC, Palo Alto, California, http://www.pymol.org, **2009**.

Received: December 18, 2009
Published online: April 22, 2010

